Observation of dynamical crater-shaped charge distribution in the space-time imaging of monolayer graphene

SCHOLARONE™
Manuscripts

Nanoscale

COMMUNICATION

Observation of dynamical crater-shaped charge distribution in the space-time imaging of monolayer graphene†

Jongweon Cho, *[a,b] Jau Tang, *[a,c] Taek Yong Hwang, [a,d] John S. Baskin [a] and Ahmed H. Zewail [§a]

A better understanding of charge carrier dynamics in graphene is key to improvement of its electronic performance. Here, we present direct space-time visualization of carrier relaxation and diffusion in monolayer graphene using time-resolved scanning electron microscopy techniques. We observed striking fluence-dependent dynamic images, changing from a Gaussian shape to a novel crater-shaped pattern with increasing laser fluence. Such direct observation of dynamic changes in spatial charge distribution is not readily available from the conventional spectroscopic approaches which reflect essentially overall effective carrier temperature and density. According to our analysis, for this crater-shaped carrier density to occur in aggregated electron-hole pairs in the high fluence regime there exists an unconventional Auger-assisted carrier recombination process to provide effective relaxation channels, most likely involving emission of optical phonons and plasmons, which is dynamically accessible due to a strong temporal overlap among them. The presented model allows us to successfully account for this unexpected phenomena and to quantitatively analyze the observed spatiotemporal behavior.

Introduction

The dynamics of charge carriers in a material accounts for a variety of physical and chemical properties, ranging from color, electrical and thermal conductivity to chemical reactivity. Optical pump-probe techniques have been widely used to investigate carrier dynamics in materials such as semiconductor nanostructures[1] and high-temperature superconductors[2]. However, such techniques usually probe the effective carrier temperature only, whereas electron imaging techniques enable direct spatial visualization of carrier dynamics at atomic scale resolution as well.[3] Ultrafast scanning electron microscopy (U-SEM), utilizing secondary electrons (SEs) detection, has been employed to study carrier dynamics of semiconductors and metals.[4-8] The inherent surface-sensitive nature of SE emission processes,[9,10] compared with the transmission-mode counterpart for bulk materials, makes it suitable for exploring such dynamics in materials that are intrinsically two-dimensional.

Monolayer graphene has a vanishing electronic density of states near K-points in reciprocal space and its linear energy-momentum dispersion represents Dirac fermions.[11] Within this framework, the dynamical behavior of hot carriers in graphene has been intensively studied. Photoexcited carriers can relax through strong carrier-carrier interactions in tens of femtoseconds, followed by slower cooling processes via electron-phonon interactions.[12-15] Other important pathways are relevant on this and longer time scales, including Auger

[a.] *Physical Biology Center for Ultrafast Science and Technology, Arthur Amos Noyes Laboratory of Chemical Physics, California Institute of Technology, Pasadena, California 91125, United States*

[b.] *Department of Physics, Myongji University, Yongin 17058, Korea. E-mail: jwcho.mju.ac.kr*

[c.] *The Institute of Technological Sciences, Wuhan University, Wuhan 0027, China. E-mail: jautang@caltech.edu*

[d.] *Molds & Dies R&D Group, Korea Institute of Industrial Technology, Bucheon 14441, Korea*

§ *Deceased*

Fig. 1 Schematic diagram of U-SEM experimental setup used in this work. The electron pulse is scanned over the surface that is illuminated with the photon pulse. The secondary electrons emitted from the sample surface are collected to construct time-resolved images at various time delays between the photon and electron pulses. For experiments involving two optical pump pulses (P$_1$ and P$_2$), the time delay between them is varied while the electron pulse is maintained at a fixed delay.

and disorder-mediated phonon scattering processes.[16-19]

Here, we report the visualization of carrier surface dynamics in monolayer graphene. We studied the U-SEM images and their dependence on laser fluence. The observation of a stark transition from Gaussian-like behavior at lower fluences to crater-shaped spatial dynamics (beginning at ~12 $\mu J/cm^2$) reveals that the non-equilibrium carrier dynamics is dominated by unconventional Auger-assisted processes. By introducing two optical pulses and one probing electron pulse, the observed images confirm such dominance in the dynamics. From our studies, a diffusion coefficient ($D \approx 6000$ cm^2/s) for surface carriers was determined and is in good agreement with previous results.[20-22] We presented a theoretical model which quantitatively reproduces all the observed results.

Results and discussion

A schematic experimental arrangement is illustrated in Fig. 1. In the current U-SEM experiments, the second harmonic (photon energy of 2.41 eV, corresponding to 515 nm wavelength, for all data) pulses of ~400 fs duration at a wavelength of 1030 nm from a Ytterbium-doped fiber laser system (Impulse by Clark-MXR) are directed to the sample at room temperature while either the fourth or the second harmonic is used to generate the pulsed photoelectrons from the field-emission gun in the SEM geometry.[10,23] Each optical pump pulse is time-delayed with respect to an electron pulse by changing the optical path via a linear translation stage. Time-resolved imaging is achieved by raster scanning the electron pulse over monolayer graphene (grown via chemical vapor deposition (CVD) and mounted on a 300-nm-thick SiO_2/Si substrate) while acquiring the emitted secondary electrons as a function of the position of the scanning electron pulse at a time delay between the optical pulse and the electron pulse. Reliable electrical contacts were made between the graphene layer and the sample holder to ensure efficient electron discharge from the sample into the electrical ground. For experiments involving two optical pump pulses (P_1 and P_2 in Fig. 1), we varied the time delay while maintaining the electron pulse at a fixed delay from P_1 (see Experimental section and Fig. S1-S2 in the ESI† for the detailed account of the experimental procedures).

Figure 2(a) shows the evolution of the U-SEM image contrast as a function of laser excitation fluence under otherwise identical experimental conditions. The difference images were constructed by subtracting the SEM images at a far negative time (where no dynamics was observed) from images at zero time delay. At low fluences, a bright single lobe on the graphene sample was observed. At higher fluences, a crater-shaped image appears with a dip in the center which becomes more pronounced as the fluence increases. The ellipticity seen in the images is due to an oblique incident
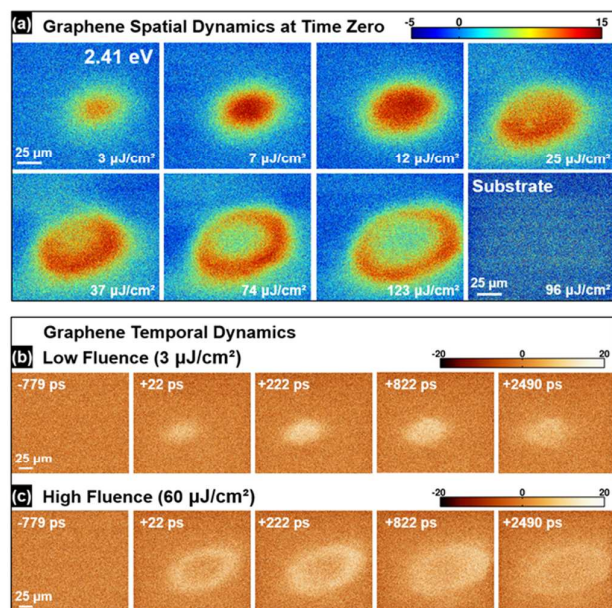
Fig. 2 Spatial and temporal dynamics of carriers in monolayer graphene. (a) U-SEM images as a function of laser excitation fluence at a 2.41 eV excitation photon energy. The difference images are obtained by subtracting the SEM images acquired at far negative time from the images recorded at zero time delay. All experimental conditions were kept identical except for the pump fluence indicated. The bottom right image is acquired on the SiO_2 substrate in the absence of the graphene layer; the same thickness of SiO_2 (300 nm) was used with and without graphene. The quadrupled harmonic (4.80 eV) is employed for electron pulse generation for all the dynamic images. (b,c) Temporal evolution of U-SEM image contrast at two representative fluences: 3 $\mu J/cm^2$ (b) and 60 $\mu J/cm^2$ (c). The second harmonic (2.41 eV) is used for the electron pulse generation.
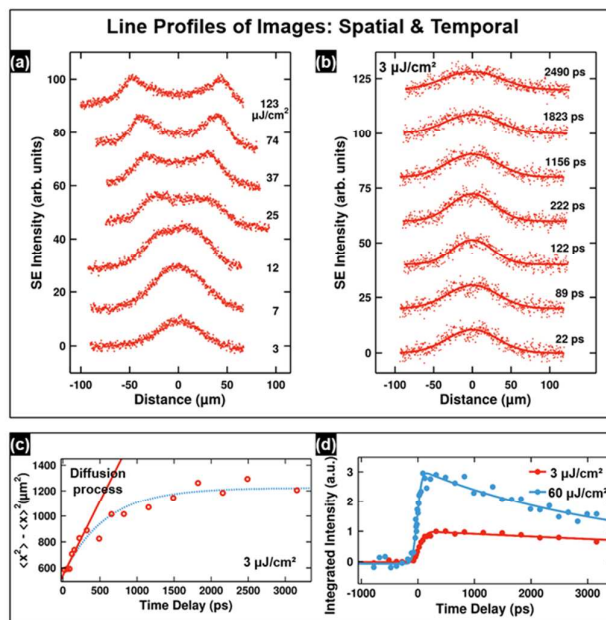
Fig. 3 Spatial, temporal line profiles and evolution of carrier population in monolayer graphene. (a) Spatial evolution of line profiles acquired along the long axis of the dynamic contrast shapes shown in Fig. 2(a); for clarity, they are displaced vertically. (b) Time evolution of line profiles along the long axis at various time delays; the laser excitation fluence is 3 $\mu J/cm^2$. For clarity, the profiles are displaced vertically. Solid lines are Gaussian fits to the data. (c) Mean square displacement (second moment) as a function of time delay obtained from data of Fig. 2(b). The dotted line denotes an empirical fit to the experimental data,† The early-time linear values give the diffusion coefficient (see Text). (d) Temporal evolution of the integrated intensities within a full field of view of the U-SEM images shown in Fig. 2(b)-(c) for the two representative fluences of 3 $\mu J/cm^2$ and 60 $\mu J/cm^2$. Solid lines are drawn as guides to the eye.

angle of ~50°. No dynamics was observed in the SiO_2 substrate with absence of graphene, as shown in the bottom right image of Fig. 2(a), indicating that this phenomenon indeed originates from the photoexcited graphene.

Further insights can be gained from the temporal evolution of images. Figure 2(b)-(c) depicts the U-SEM images acquired at various time delays for two representative pump fluences of 3 and 60 μJ/cm^2, respectively. At negative time delays, when the electron pulse precedes the photon pulse, we did not observe significant image contrast changes. Near time zero, a single-lobed Gaussian-like behavior was observed at 3 μJ/cm^2, but at the higher fluence of 60 μJ/cm^2, the crater-like pattern appeared which gradually diminished at longer times due to diffusion.

A series of spatial "line profiles" taken along the long axis of the elliptical contrast shown in Fig. 2(a) provides a clear trend, as depicted in Fig. 3(a). A Gaussian profile is noticeable at low-fluence excitation and becomes flattened for intermediate-fluence values, with a crater shape emerging at higher fluences. A crossover of the contrast change was observed to occur at 12-15 μJ/cm^2.

The temporal "line profiles" reveal how the U-SEM images evolves with time. Fig. 3(b) shows the temporal evolution of the spatial distribution along the long axis of the contrast at various time delays and for the excitation fluence of 3 μJ/cm^2. Gaussian fits to the data are shown in red solid lines. In this case, the width, also expressed as the square root of the second moment, clearly increases with time, providing a measure of the diffusion coefficient. Figure 3(c) displays the values for the second moment obtained from Fig. 3(b) which exhibits a linear time dependence at short times and then reaches an asymptotic value at later times. Values of the diffusion coefficient are given in the following section.

Finally, Fig. 3(d) displays the spatially-integrated U-SEM image intensities at two fluences (obtained from Fig. 2(b)-(c)) as a function of time delays. The total number of carriers remains nearly unchanged for the lower fluence (3 μJ/cm^2) but for the higher fluence (60 μJ/cm^2) there is a definite decay that begins after ~150 ps. A rise time of monolayer graphene is not limited by the instrumentation response (Fig. S3(a)-(b)†). The electrons in graphene excited by ultrafast optical pulses are known to thermalize primarily through carrier-carrier scattering resulting in a well-defined Fermi-Dirac distribution on a timescale of the order of <100 fs.[13-15] The temporal resolution deduced from the instrumentation response of our apparatus for this work is ~1.2 ps (Fig. S3(a)†) which is insufficient to undoubtedly resolve when the crater-shaped spatial distribution starts to develop and further infer possible effects associated with carrier thermalization.[24] We do not observe a crossover between single-lobed and crater-shaped features during the recovery processes.

The most striking and unexpected feature of our experimental observation is the emergence of crater-shaped U-SEM images at relatively high excitation fluences. The crucial and pertinent question is what could possibly be the mechanism that gives rise to the observed crossover in the U-SEM images. We have ruled out Rabi oscillations as a possible

origin: First of all, a second oscillation was not observed when the excitation fluence was successively increased. Secondly, in experiments involving two pump-pulse excitation with the same color (515 nm), the crater-type contrast pattern persists even at a longer time delay of 13 ps between the two pump pulses (see Fig. S4). This by itself rules out the Rabi mechanism, because the carriers dephasing time in monolayer graphene is ~85 fs.[25] Other scenarios, including a saturation effect, were also considered but excluded (see Experimental section, control experiments, for a detailed discussion).

Here, we propose a kinetic model to account for all observations made. Figure S5 illustrates an e-h pair kinetic scheme involving three states.† In the Fig. S5, w denotes an optical pumping rate for a single e-h pair excitation. Optical excitation of an additional e-h pair, in close proximity but spatially uncorrelated to the one e-h pair state, can form a two e-h pair state (Fig. S5(b)†). This two e-h pair state can either (i) relax to a single e-h pair state through conventional Auger recombination and subsequent energy-momentum relaxation (denoted as α) or (ii) directly transit into the ground state through an Auger-assisted channel, primarily involving emission of optical phonons and plasmons (denoted as β). In our model local populations of these pair states effectively constitute the U-SEM image intensity.

One key mechanism in our model responsible for the crater-shaped U-SEM images at high fluences is the direct relaxation channel from the two pair state to the ground state. Based on our model simulations this mechanism leads to the observed crater-shaped behavior (Fig. S6(a)†). Conventional Auger recombination is a result of Coulomb interactions among multiple carriers involving nonradiative annihilation of an e-h pair followed by the transfer of the excess energy to other carriers.[26] Such a mechanism is important for small bandgap semiconductors,[27] but this mechanism alone would only create a flat-top spatial distribution for the U-SEM image, not leading to a central dip in the e-h pair-density distribution. This simple kinetic model involving a relaxation pathway from the two e-h pair state to the single e-h pair state (i.e., β = 0) is able to reproduce the flat-top U-SEM spatial profile attainable from a rate equation involving the conventional carrier-density-dependent Auger recombination. According to our systematic simulations, β plays a decisive role in the formation and fluence-dependent behavior of such crater-shaped features, whereas α plays a minor role (Fig. S6-S7†).

Auger-type processes in monolayer graphene has garnered substantial attention,[16-18,28] primarily due to the vanishing energy gap and linear band dispersion in the vicinity of the Dirac point. Among those of particular interest is impact ionization (or inverse Auger recombination), where an additional e-h pair is created as a consequence of the Coulomb-induced relaxation of hot carriers. It was proposed that the process would lead to a substantial enhancement in carrier multiplication in graphene.[18,29] Our observation of a crater-shaped charge distribution, reflecting an intensity dip at sufficiently large fluences, is inconsistent with the prediction from this carrier multiplication mechanism, as it would lead to an increase rather than a decrease in the e-h pair population.

Moreover, while the impact ionization occurring at low excitation fluences may contribute to the overall enhancement of the detected intensities at ultrafast time scales (<100 fs), it is theoretically predicted to be less pronounced in the strong optical excitation regime we considered here.[18,29]

Phonon emission plays a pivotal role in carrier relaxation in graphene. The zone-center optical phonons (E_{2g} modes) are responsible for intra-valley interband transitions, whereas the zone-edge phonons (A_1' modes) contribute to inter-valley interband recombination. The effective reduction in available phase space for carriers, due to the 2D nature of monolayer graphene with zero bandgap, leads to enhanced Coulomb interactions when compared to bulk semiconductors. The Coulomb-enabled Auger recombination processes create a significant population of transient carriers in higher-lying electronic states and lead to broadened electron-energy distributions. Considering the large optical phonon energies (~200 meV)[30] and linear energy dependence of electronic density of states in monolayer graphene, the "Auger heating" processes may enable efficient e-h recombination when they are dynamically coupled to other energetically accessible channels such as emission of multiple, anisotropic optical phonons.[31,32]
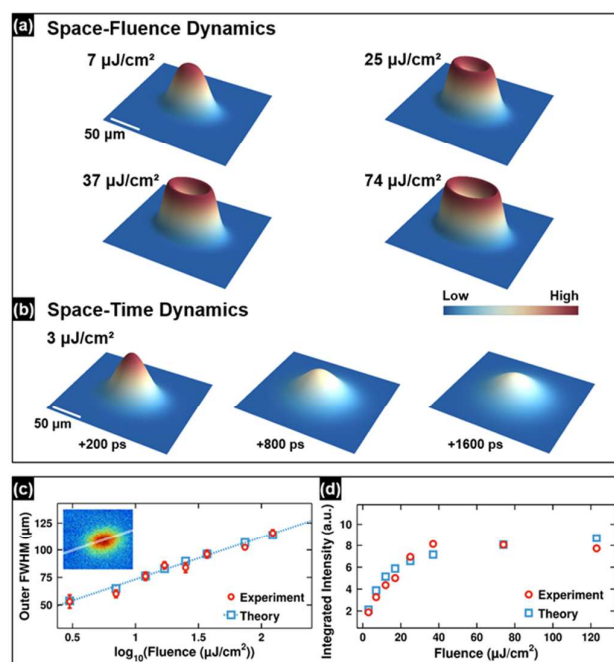
Fig. 4 Theoretical modeling results of space-fluence and space-time carrier dynamics in monolayer graphene, and comparison with the experimental results. (a) Shown in three-dimensional plots are U-SEM image intensities at various fluences and at zero time delay. (b) U-SEM image intensities at various time delays for 3 μJ/cm². The results capture the key spatial, fluence-dependent, and temporal behavior seen in the experimental data. (c) FWHM along the long axis of the imaged features shown in Fig. 2(a) as a function of the pump fluence. Red empty circles and blue empty squares indicate the experimental and theoretical values, respectively. The inset depicts a stripe over the U-SEM image (7 μJ/cm²) that was used to extract the values, as an example. The dotted line is the least square fit to the theoretical prediction. (d) Integrated intensities for the images shown in Fig. 2(a) as a function of pump fluence. Red empty circles and blue empty squares indicate the experimental and simulated results, respectively. The key parameters used in our model are given in Table S1.†

The photoexcited carrier densities of the results shown in Fig. 2(a) are estimated to be in the range of 10^{11} to 4×10^{12} cm^{-2} based on the optical absorption of graphene and the illumination geometry in our experiments.[33,34] While Auger processes in conventional semiconductors, such as a submicron Si film on a sapphire substrate,[35] occur on a time scale of hundreds of ps or even longer, which is orders of magnitude slower than emission of optical phonons in such materials, the gapless electronic spectrum and perfect carrier confinement of graphene make the time scales closer for these two mechanisms; theoretical calculations by Rana *et al.* predicted carrier recombination times induced by emission of optical phonons[36] and Auger processes[37] to be a few ps at room temperature near the crossover of the spatial contrast shape transition. Furthermore, carrier recombination through plasmon emission over our carrier-density range becomes dominant over the carrier generation counterpart.[38] Because of a strong temporal overlap between Auger recombination and emissions of phonons and plasmons, in contrast to the conventional semiconducting materials, new dynamical channels become accessible for hot carriers to cool down efficiently. In such cases, it is possible to involve both interband and intraband carrier relaxations due to their ultrafast timescale.[39]

Figure 4(a)-(b) shows three-dimensional plots of the evolution of simulated U-SEM image intensity distributions, which are related to the electron density,† as a function of fluence at zero time delay [Fig. 4(a)] and at later times for a representative excitation fluence of 3 μJ/cm² [Fig. 4(b)]. Our simulation results capture the distinctive change from a single Gaussian lobe to crater-shaped feature as observed experimentally [Fig. 2(a)] with its temporal evolution [Fig. 2(b)-(c)].

Furthermore, fluence-dependent spatial extent and integrated intensities of the simulated image intensity profiles at various time delays are in good agreement with those obtained from the experimental data. We found that the spatial extent and integrated intensities of the bright-contrast regions increase with laser fluence. Figure 4(c) shows a full width at half maxima (FWHM), for the cross section along a long axis of the feature, as a function of the pump fluence on a semi-log scale. The FWHM clearly exhibits a linear relationship with a logarithmic increase of the pump fluence.

Figure 4(d) displays the pump fluence dependence of the integrated U-SEM image intensity over a full field of view of the images shown in Fig. 2(a). At low fluence, the intensities show a linear increase and become nearly saturated at high enough fluences. The overall magnitude of the intensity is larger for the high fluence than that for the low fluence, consistent with the temporal behavior from experiments [Fig. 3(d)] and simulations (Fig. S8†). The simulated results capture the key fluence-dependent and temporal behavior seen in the experimental data; nevertheless, small deviation from the experimental observations is likely due to the simple treatment of the decay rate parameters used in our model.

The evolution of the spatial charge profile in time provides further information about how photoexcited carriers diffuse

away from the illuminated region. In Fig. 3(c), at the excitation fluence of 3 μJ/cm^2, the least square fit to the initial data points (<450 ps) yields a diffusion coefficient of (5.8±0.7)x10^3 cm^2/s. This value compares well with the reported experimental diffusion coefficient for CVD-grown graphene[21] and approximately a factor of two smaller than that of epitaxial graphene,[20] let alone that of free-standing graphene calculated using Monte-Carlo simulations.[22] The agreement is good considering the different graphene growth techniques.

Conclusions

Using U-SEM the ultrafast carrier dynamics, such as carrier relaxation and diffusion, in monolayer graphene are visualized in real space and time. We observed striking crater-shaped U-SEM images at high optical-excitation fluences. To the best of our knowledge, such a phenomenon has not been reported before. This demonstrates the advantage of directly imaging local charge distribution in time, in contrast to the conventional all-optical pump-probe technique which usually provides mixed information about carrier temperature and density. This study uncovers that the spatiotemporal evolution is mainly due to an efficient, unconventional Auger-assisted relaxation process, most likely involving emission of optical phonons and plasmons that becomes dynamically accessible only at high pump fluences. So far, the crater-type carrier dynamics is found to be unique to graphene and was not observed in silicon or metals. The experimental approach, with the simple theoretical model discussed here, offers a consistent explanation for the observations, suggesting possible extension of U-SEM to other 2D layered materials, ultrathin films or surfaces of bulk materials.

Experimental section

Methods

Our experimental setup utilizes the secondary electrons, generated by an electron pulse in the SEM, as probe signals. In this scheme, time-dependent changes in secondary electron yield of a graphene sample induced by an optical pump pulse are measured and used to construct images. U-SEM images present the spatial variation of difference in SEM image intensities where SEM images acquired at a specific time delay between an optical pulse and electron pulse were referenced to the images acquired at far negative time where no detectable dynamics was observed. As such, only dynamic signals constitute the images, as static signals are subtracted. The emitted secondary electrons are replenished by a good contact between the sample and the electrical ground via copper clips or conductive glue. Line-scan images at sample surfaces exhibited no substantial intensity variations, indicating negligible charging effects during data acquisition.

The samples were positioned at a working distance of 10 mm and perpendicular to the propagation direction of the pulsed electron beam, with its energy of 30 keV. The emitted electrons from the sample surface were collected using a positively-biased Everhart-Thornley detector. Our experiments rely on stroboscopic recording of images and full recovery of the sample's dynamical response was ensured before the arrival of a next pump pulse. At each delay, the synchronization between the optical pump pulse and the electron pulse is ensured at every pixel. All U-SEM images (512x442 pixels) were acquired at a dwell time of 1 μs per pixel, indicating the time span between the measurements on two neighboring pixels is 1 μs, and were integrated 64 times to improve the signal-to-noise ratio. The pulse energy of an electron-generating laser beam was ~3 nJ. A repetition rate of 8.4 MHz was used to ensure full recovery of graphene dynamics and for signal-to-noise ratio optimization. The scheme of excitation and electron liberation is shown in Fig. S1(a).

For an identical laser system (Clark-MXR, Impulse), we have obtained measurements of the beam shape and for the two vertical positions; the beam is Gaussian-type over the power range of <1 mW to ~300 mW [Fig. S1(b)]. Since inserting a neutral density (ND) filter in the beam does not change a transverse mode of the laser beam, we inserted a ND filter in the beam path in U-SEM measurements to ensure whether the crater-shaped feature is robust at high fluences. By simply inserting the ND filter into the beam path, the crater shape disappeared. With this experiment, we confirmed that the beam shape was not responsible for our observations, as also shown in Fig. S1(b).

Monolayer graphene samples, purchased from Graphene Supermarket, were grown via CVD techniques and then transferred onto SiO$_2$ (300 nm)/Si substrates. We characterized the graphene specimen using optical imaging and Raman spectroscopy.[40-42] Figure S2(a) is an optical micrograph of the investigated graphene sample, revealing a relatively homogenous sample appearance with few defects and dislocations. Figure S2(b) shows typical Raman spectra acquired on the investigated samples using a Renishaw inVia Raman microscope at room temperature in ambient conditions with 514 nm light irradiation at low power. The presence of D-, G-, and 2D-peaks at 1346, 1589, and 2691 cm^{-1}, respectively, together with the Lorentzian-fitted 2D peak shown in the inset of Fig. S2(b), indicates the graphene characteristics; this would not be the case for multilayer graphite.[41] The ratios of D- to G-peak and G- to 2D-peak are ~0.3 and ~0.4, respectively, also suggesting the predominant presence of a single layer of graphene. [40-42]

To ensure that the rise time in graphene is not limited by the instrumentation response, we performed independent measurements on p-type Si(100) (purchased from MTI) under the identical experimental conditions used for the graphene study, except for the pump laser fluence (~0.6 mJ/cm^2). We obtained a transient U-SEM image intensity showing a rise time of 1.2±0.2 ps [see Fig. S3(a)], as compared to that of monolayer graphene which gives 52±3 ps [see Fig. S3(b)] at the center spot. In addition, we do not observe a crossover between a single lobe and crater-shaped feature during the recovery processes.

Control experiments

We observed no U-SEM contrast change in the SiO_2 substrate in the absence of the graphene layer [bottom right image of Fig. 2(a)]; the same thickness of SiO_2 (300 nm) was used with and without graphene. This result indicates that the U-SEM images arise solely from graphene. We note that the fluence threshold for a single-shot multiphoton ionization[43] of SiO_2 (bandgap of ~9 eV) is four orders of magnitude larger than the laser fluence used in our experiments, thus excluding the influence of such processes.

We also note that the fluence needed to induce crater-shaped U-SEM signals in monolayer graphene is more than 4 orders of magnitude lower than the reported single-shot damage threshold under intense femtosecond laser exposure.[44,45] The experimental data are reproducible on the same sample area. This was confirmed by the fact that no appreciable changes in the dynamic features (including a crater-shaped pattern) were seen when successive data sets were compared. Moreover, there was no apparent damage found in the images acquired during data acquisition at the highest laser fluence and at the end of measurements, further indicating that the measured contrast is not caused by structural damage. Similarly, the temperature rise of graphene is insignificant because of its very high thermal conductivity (>1500 W/m·K for CVD-monolayer graphene[46]). At a fluence of 15 μJ/cm^2 the temperature rise is ~2 K and at the highest fluence used of 123 μJ/cm^2, the rise is ~20 K.[47,33,34]

Prior studies of non-thermal carrier dynamics in prototypical semiconducting materials using the U-SEM technique in this laboratory revealed that the bright contrast in images arises from the enhancement of the secondary electron emissions upon the arrival of an electron pulse, resulting from an energy gained by transient conduction electrons through optically-excited interband electronic transition.[5,6,8] The differences in the U-SEM image intensities referenced to unilluminated surface areas thus reflect the changes in the transient population of conduction band electrons. While an intricate interplay between the energy gain and photo-assisted energy loss mechanisms may lead to a bright and/or dark contrast in other materials,[6] monolayer graphene is atomically thin, and does not exhibit any discernible dynamics at negative time delays, as shown in Fig. 2(b)-(c) and 3(d). Moreover, the U-SEM signal remains as a bright contrast at positive time delays, including a contrast dip in the center of the donut-like footprint observed at high fluences. Therefore, we attribute our observations of the fluence-dependent changes in the contrast patterns to the optically excited electron-hole (e-h) pairs through dipole-allowed π- π* transitions and their relaxation back to the ground state, which provides detailed insights into efficient dynamical relaxation channels that are strongly dependent on the fluence of the irradiation.

We emphasize that the observed transition of the spatial intensity takes place at excitation fluences by more than 40 times lower than those for absorption saturation in monolayer graphene[48] and by orders of magnitude lower than those for stimulated emission observed in this material.[49] Furthermore, a previous experimental observation of radiative e-h recombination in monolayer graphene revealed a quantum efficiency as low as ~10^{-9},[50] suggesting that the observed dynamics in this work should involve strong fluence-dependent carrier recombination channels other than radiative processes.

The saturation limit of the Everhart-Thornley detector in our apparatus was determined by a linear response behavior in the U-SEM images.[51] At the highest sensitivity the limit corresponds to a maximum ~8 electrons per pixel at the detector, with a dwell time of 1 μs. A pixel is about 415 nm (while the spatial resolution achievable with the apparatus used in his work is ~10 nm[4], the evolution of the fluence-dependent spatial charge profile is most discernible when the field of view is comparable to the size of the pump beam, so we resort to this length scale here). An estimate of the number of electrons per pixel in our experiments is less than 6 at the highest sensitivity. Thus, all experiments were conducted below the saturation limit. The laser beam shape was kept unchanged with excitation fluence. Additionally, we observed the consistent dynamic features even when the samples were ex-situ annealed up to ~250 °C.

We note that the polycrystalline nature of CVD graphene is known to have a sizeable influence on carrier scattering and thus mobility.[52] Despite our efforts on 4D carrier mapping over many different sample areas, no statistically significant anisotropy was found, possibly due to an insufficient signal-to-noise ratio for imaging in both space and time.

Conflicts of interest

There are no conflicts to declare.

Acknowledgements

References

1   J. Shah, *Ultrafast Spectroscopy of Semiconductors and Semiconductor Nanostructures*, Springer, Germany, 1996.
2   J. Orenstein, *Phys. Today* 2012, **65**, 44.
3   A. H. Zewail, *Science* 2010, **328**, 187.

COMMUNICATION

4   D. S. Yang, O. F. Mohammed, A. H. Zewail, *Proc. Natl. Acad. Sci. U.S.A.* 2010, **107**, 14993.

5   O. F. Mohammed, D. S. Yang, S. K. Pal, A. H. Zewail, *J. Am. Chem. Soc.* 2011, **133**, 7708.

6   J. Cho, T. Y. Hwang, A. H. Zewail, *Proc. Natl. Acad. Sci. U.S.A.* 2014, **111**, 2094.

7   J. Sun, V. A. Melnikov, J. I. Khan, O. F. Mohammed, *J. Phys. Chem. Lett.* 2015, **6**, 3884.

8   J. Sun, A. Adhikari, B. S. Shaheen, H. Yang, O. F. Mohammed, *J. Phys. Chem. Lett.* 2016, **7**, 985.

9   L. Reimer, *Scanning electron microscopy: physics of image formation and microanalysis*, Springer, Berlin, ed. 2, 1998.

10   H. Seiler, *J. Appl. Phys.* 1983, **54**, R1.

11   A. H. Castro Neto, F. Guinea, N. M. R. Peres, K. S. Novoselov, A. K. Geim, *Rev. Mod. Phys.* 2009, **81**, 109.

12   R. W. Newson, J. Dean, B. Schmidt, H. M. van Driel, *Opt. Express* 2009, **17**, 2326.

13   M. Breusing, S. Kuehn, T. Winzer, E. Malic, F. Milde, N. Severin, J. P. Rabe, C. Ropers, A. Knorr, T. Elsaesser, *Phys. Rev. B* 2011, **83**, 153410.

14   H. N. Wang, J. H. Strait, P. A. George, S. Shivaraman, V. B. Shields, M. Chandrashekhar, J. Hwang, F. Rana, M. G. Spencer, C. S. Ruiz-Vargas, J. Park, *Appl. Phys. Lett.* 2010, **96**, 081917.

15   J. C. Johannsen, S. Ulstrup, F. Cilento, A. Crepaldi, M. Zacchigna, C. Cacho, I. C. E. Turcu, E. Springate, F. Fromm, C. Raidel, T. Seyller, F. Parmigiani, M. Grioni, P. Hofmann, *Phys. Rev. Lett.* 2013, **111**, 027403.

16   D. Brida, A. Tomadin, C. Manzoni, Y. J. Kim, A. Lombardo, S. Milana, R. R. Nair, K. S. Novoselov, A. C. Ferrari, G. Cerullo, M. Polini, *Nat. Commun.* 2013, **4**, 1987.

17   I. Gierz, J. C. Petersen, M. Mitrano, C. Cacho, I. C. E. Turcu, E. Springate, A. Stohr, A. Kohler, U. Starke, A. Cavalleri, *Nat. Mater.* 2013, **12**, 1119.

18   T. Winzer, A. Knorr, E. Malic, *Nano Lett.* 2010, **10**, 4839.

19   J. C. W. Song, M. Y. Reizer, L. S. Levitov, *Phys. Rev. Lett.* 2012, **109**, 106602.

20   B. A. Ruzicka, S. Wang, L. K. Werake, B. Weintrub, K. P. Loh, H. Zhao, *Phys. Rev. B* 2010, **82**, 195414.

21   B. A. Ruzicka, S. Wang, J. W. Liu, K. P. Loh, J. Z. Wu, H. Zhao, *Opt. Mater. Express* 2012, **2**, 708.

22   R. Rengel, M. J. Martin, *J. Appl. Phys.* 2013, **114**, 143702.

23   P. L. Gai, E. D. Boyes, *Electron Microscopy in Heterogeneous Catalysis*, CRC Press, 2003.

24   W. H. Knox, C. Hirlimann, D. A. B. Miller, J. Shah, D. S. Chemla, C. V. Shank, *Phys. Rev. Lett.* 1986, **56**, 1191.

25   P. N. Romanets, F. T. Vasko, *Phys. Rev. B* 2010, **81**, 241411(R).

26   S. M. Sze, *Physics of Semiconductor Devices*, Wiley, Hoboken, New Jersey, ed. 3, 2007.

27   P. Harrison, *Quantum Wells, Wires and Dots*, Wiley, New York, ed. 2, 2005.

28   K. J. Tielrooij, J. C. W. Song, S. A. Jensen, A. Centeno, A. Pesquera, A. Z. Elorza, M. Bonn, L. S. Levitov, F. H. L. Koppens, *Nat. Phys.* 2013, **9**, 248.

29   T. Winzer, E. Malic, *Phys. Rev. B* 2012, **85**, 241404(R).

30   J. K. Viljas, T. T. Heikkila, *Phys. Rev. B* 2010, **81**, 245404.

31   C. H. Park, F. Giustino, J. L. McChesney, A. Bostwick, T. Ohta, E. Rotenberg, M. L. Cohen, S. G. Louie, *Phys. Rev. B* 2008, **77**, 113410.

32   D. M. Basko, *Phys. Rev. B* 2013, **87**, 165437.

33   R. R. Nair, P. Blake, A. N. Grigorenko, K. S. Novoselov, T. J. Booth, T. Stauber, N. M. R. Peres, A. K. Geim, *Science* 2008, **320**, 1308.

34   T. Stauber, N. M. R. Peres, A. K. Geim, *Phys. Rev. B* 2008, **78**, 085432.

35   M. C. Downer, C. V. Shank, *Phys. Rev. Lett.* 1986, **56**, 761.

36   F. Rana, P. A. George, J. H. Strait, J. Dawlaty, S. Shivaraman, M. Chandrashekhar, M. G. Spencer, *Phys. Rev. B* 2009, **79**, 115447.

37   F. Rana, *Phys. Rev. B* 2007, **76**, 155431.

38   F. Rana, J. H. Strait, H. N. Wang, C. Manolatou, *Phys. Rev. B* 2011, **84**, 045437.

39   J. M. Hamm, A. F. Page, J. Bravo-Abad, F. J. Garcia-Vidal, O. Hess, *Phys. Rev. B* 2016, **93**, 041408(R).

40   A. C. Ferrari, J. C. Meyer, V. Scardaci, C. Casiraghi, M. Lazzeri, F. Mauri, S. Piscanec, D. Jiang, K. S. Novoselov, S. Roth, and A. K. Geim, *Phys. Rev. Lett.* 2006, **97**, 187401.

41   M. S. Dresselhaus, A. Jorio, M. Hofmann, G. Dresselhaus, and R. Saito, *Nano Lett.* 2010, **10**, 751.

42   A. Das, S. Pisana, B. Chakraborty, S. Piscanec, S. K. Saha, U. V. Waghmare, K. S. Novoselov, H. R. Krishnamurthy, A. K. Geim, A. C. Ferrari, and A. K. Sood, *Nature Mater.* 2008, **3**, 210.

43   D. Grojo, M. Gertsvolf, S. Lei, T. Barillot, D. M. Rayner, and P. B. Corkum, *Phys. Rev. B* 2010, **81**, 212301.

44   A. Roberts, D. Cormode, C. Reynolds, T. Newhouse-Illige, B. J. Leroy, and A. S. Sandhu, *Appl. Phys. Lett.* 2011, **99**, 051912.

45   H. O. Jeschke, M. E. Garcia, and K. H. Bennemann, *Phys. Rev. Lett.* 2001, **87**, 015003.

46   A. A. Balandin, *Nature Mater.* 2011, **10**, 569.

47   A maximum rise in the lattice temperature at the center of illuminated spot on a graphene layer is estimated in a single shot regime, using ~1.24 % optical absorption (refs. 33, 34) at an incidence angle of 50° (by correcting for the reflection), a mass density of 7.6×10^{-8} g/cm^2 and a heat capacity of 0.7 J/g·K.

48   T. Winzer, A. Knorr, M. Mittendorff, S. Winnerl, M. B. Lien, D. Sun, T. B. Norris, M. Helm, and E. Malic, *Appl. Phys. Lett.* 2012, **101**, 221115.

49   T. Li, L. Luo, M. Hupalo, J. Zhang, M. C. Tringides, J. Schmalian, and J. Wang, *Phys. Rev. Lett.* 2012, **108**, 167401.

50   C. H. Lui, K. F. Mak, J. Shan, and T. F. Heinz, *Phys. Rev. Lett.* 2010, **105**, 127404.

51   D.-S. Yang, O. F. Mohammed, and A. H. Zewail, *Angew. Chem. Int. Ed.* 2013, **52**, 2897.

52   K. Kim, Z. Lee, W. Regan, C. Kisielowski, M. F. Crommie, and A. Zettl, *ACS Nano* 2011, **5**, 2142.